

Article

Low-Dimensional Architectures in Isomeric *cis*-PtCl₂{Ph₂PCH₂N(Ar)CH₂PPh₂} Complexes Using Regioselective-N(Aryl)-Group Manipulation

 Peter De'Ath, Mark R. J. Elsegood , Noelia M. Sanchez-Ballester and Martin B. Smith *

Department of Chemistry, Loughborough University, Loughborough LE11 3TU, UK; P.DeAth@lboro.ac.uk (P.D.); m.r.j.elsegood@lboro.ac.uk (M.R.J.E.); n.m.sanchez-ballester@lboro.ac.uk (N.M.S.-B.)

* Correspondence: m.b.smith@lboro.ac.uk

Abstract: The solid-state behaviour of two series of isomeric, phenol-substituted, aminomethylphosphines, as the free ligands and bound to Pt^{II}, have been extensively studied using single crystal X-ray crystallography. In the first library, isomeric diphosphines of the type Ph₂PCH₂N(Ar)CH₂PPh₂ [**1a–e**; Ar = C₆H₃(Me)(OH)] and, in the second library, amide-functionalised, isomeric ligands Ph₂PCH₂N{CH₂C(O)NH(Ar)}CH₂PPh₂ [**2a–e**; Ar = C₆H₃(Me)(OH)], were synthesised by reaction of Ph₂PCH₂OH and the appropriate amine in CH₃OH, and isolated as colourless solids or oils in good yield. The non-methyl, substituted diphosphines Ph₂PCH₂N{CH₂C(O)NH(Ar)}CH₂PPh₂ [**2f**, Ar = 3-C₆H₄(OH); **2g**, Ar = 4-C₆H₄(OH)] and Ph₂PCH₂N(Ar)CH₂PPh₂ [**3**, Ar = 3-C₆H₄(OH)] were also prepared for comparative purposes. Reactions of **1a–e**, **2a–g**, or **3** with PtCl₂(η⁴-cod) afforded the corresponding square-planar complexes **4a–e**, **5a–g**, and **6** in good to high isolated yields. All new compounds were characterised using a range of spectroscopic (¹H, ³¹P{¹H}), FT-IR) and analytical techniques. Single crystal X-ray structures have been determined for **1a**, **1b**·CH₃OH, **2f**·CH₃OH, **2g**, **3**, **4b**·(CH₃)₂SO, **4c**·CHCl₃, **4d**·½Et₂O, **4e**·½CHCl₃·½CH₃OH, **5a**·½Et₂O, **5b**, **5c**·½H₂O, **5d**·Et₂O, and **6**·(CH₃)₂SO. The free phenolic group in **1b**·CH₃OH, **2f**·CH₃OH, **2g**, **4b**·(CH₃)₂SO, **5a**·½Et₂O, **5c**·½H₂O, and **6**·(CH₃)₂SO exhibits various intra- or intermolecular O–H···X (X = O, N, P, Cl) hydrogen contacts leading to different packing arrangements.

Keywords: amide groups; isomers; late-transition metals; P-ligands; phenols; secondary interactions; single crystal X-ray crystallography



Citation: De'Ath, P.; Elsegood, M.R.J.; Sanchez-Ballester, N.M.; Smith, M.B. Low-Dimensional Architectures in Isomeric *cis*-PtCl₂{Ph₂PCH₂N(Ar)CH₂PPh₂} Complexes Using Regioselective-N(Aryl)-Group Manipulation. *Molecules* **2021**, *26*, 6809. <https://doi.org/10.3390/molecules26226809>

Academic Editors: William T. A. Harrison, R. Alan Aitken and Paul Waddell

Received: 28 September 2021
Accepted: 7 November 2021
Published: 11 November 2021

Publisher's Note: MDPI stays neutral with regard to jurisdictional claims in published maps and institutional affiliations.



Copyright: © 2021 by the authors. Licensee MDPI, Basel, Switzerland. This article is an open access article distributed under the terms and conditions of the Creative Commons Attribution (CC BY) license (<https://creativecommons.org/licenses/by/4.0/>).

1. Introduction

Tertiary phosphines, and their phosphine oxides, have played an important role in the study of supramolecular and self-assembly processes [1–3]. Their synthetic versatility, coupled with ease of substituent modification, has no doubt played a significant contribution over the years. Hydrogen bonding interactions are routinely encountered in supramolecular ligand systems as illustrated by the elegant studies from Breit [4], Reek [5], and others [6,7]. More recently, amongst other common types of non-covalent interactions, those based on halogen bonding [8,9] and H^{δ+}···H^{δ−} have been reported [10].

For a number of years, we [11–16], and others [17–22], have been interested in aminomethylphosphines, readily amenable by Mannich condensation reactions. Such interest stems from the relative ease of accessing *P*-monodentate ligands based on a P–C–N linker [11,15,16,19,20,22] or *P/P*-bidentate derivatives bearing a P–C–N–C–P backbone [12–14,17–19,21]. Previously, we have shown that the N-arene group can be easily tuned with, for example, various H-bonding donor/acceptor sites based on –CO₂H/OH groups [12–16]. In continuation of these studies, we report here our work on the regioselective positioning of amide/hydroxy and methyl groups within a series of aminomethylphosphines, both as the free ligands and when coordinated to a square-planar Pt(II) metal centre. Our rationale for introducing an –C(O)NH– group is based on the known use of

this functionality in supramolecular chemistry [23] and, furthermore, the recent interest in amide-modified phosphines for their variable coordination chemistry [24–26], binding nitroaromatics [27], and relevance to catalysis based on Pd [28]. Our choice of metal fragment in this work, “*cis*-PtCl₂”, is based on its capability to support a relatively small bite angle diphosphine ligand in a *cis*, six-membered ring conformation, and to provide up to two “acceptor” sites for potential H-bonding [29]. For this purpose, we elected to pursue a double Mannich condensation reaction of Ph₂PCH₂OH with a series of isomeric primary amines bearing either OH/CH₃ groups and/or an amide spacer between the arene and P–C–N–C–P backbone (Chart 1).

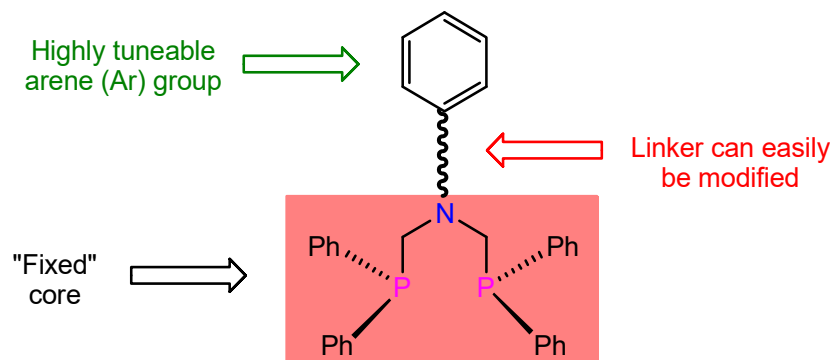
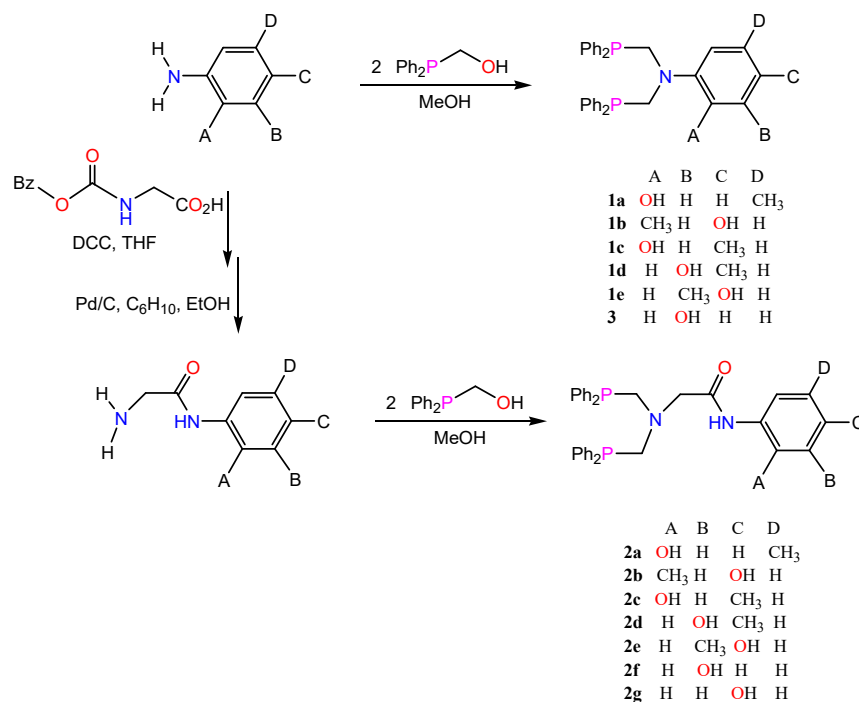


Chart 1. Potential modification sites of a Ph₂P–C–N(Ar)–C–PPh₂ backbone.

2. Results and Discussion

2.1. Ligand Synthesis

We [11–16,29], and others [17,19–22], have previously used Mannich condensations as a versatile method for the synthesis of aminomethylphosphines. Accordingly, two equivalents of Ph₂PCH₂OH were reacted with one equivalent of the amine, for 24 h at r.t. under N₂, yielding the desired phenol-substituted ditertiary phosphines **1a–e** and **3** (Scheme 1).



Scheme 1. Synthesis of **1a–e**, **2a–g**, and **3**.

For **1a–e**, colourless solids were isolated in 38–97% yields and found to be air stable in the solid state, but oxidise rapidly in solution. Compounds **1a–e** and **3** exhibit single resonances in their $^{31}\text{P}\{^1\text{H}\}$ NMR spectra (in d^6 -dmsO) around $\delta(\text{P}) -26$ ppm [12–15,29], indicating the presence of only one P^{III} environment. The ligands were also characterised by ^1H NMR, FT-IR, and elemental analysis (Table 1). In particular, the absence of an NH resonance, in the ^1H NMR spectra, confirmed that double condensation had occurred.

Table 1. Selected spectroscopic and analytical data for compounds **1a–3** ^a.

Compound ^a	$\delta(\text{P})$ ^b	$\delta(\text{H})$ /OH (NH)	$\delta(\text{H})$ /arom. H.	$\delta(\text{H})$ /CH ₂	$\delta(\text{H})$ /CH ₂ ^d	$\delta(\text{H})$ /CH ₃	ν_{OH} (ν_{NH}) ^e	Microanalysis (CHN)
1a (79)	−27.5	8.62	7.33–7.23, 6.76, 6.69–6.57		4.15 (2.4)	2.10	3398	Calc. for C ₃₃ H ₃₁ NOP ₂ , C, 76.29; H, 6.01; N, 2.70 Found, C, 76.07; H, 6.13; N, 2.78
1b (56)	−27.3	9.06	7.36–7.26, 7.15, 6.50, 6.44		3.96 (5.6)	1.74	3282	Calc. for C ₃₃ H ₃₁ NOP ₂ .2MeOH, C, 72.03; H, 6.74; N, 2.40 Found, C, 72.45; H, 6.04; N, 2.58
1c (97)	−27.5	8.77	7.44–7.22, 6.86, 6.54, 6.48		4.09 (3.4)	2.12	3389	Calc. for C ₃₃ H ₃₁ NOP ₂ , C, 76.29; H, 6.01; N, 2.70 Found, C, 75.99; H, 6.00; N, 2.76
1d (38)	−26.7	8.63	7.40–7.30, 6.55		4.02 (3.2)	1.96	3432	Calc. for C ₃₃ H ₃₁ NOP ₂ , C, 76.29; H, 6.01; N, 2.70 Found, C, 75.53; H, 6.05; N, 2.74
1e (96)	−26.4	9.06	7.49–7.33, 6.85, 6.50, 6.27		3.88 (3.6)	2.08	3387	Calc. for C ₃₃ H ₃₁ NOP ₂ .MeOH, C, 74.03; H, 6.40; N, 2.54 Found, C, 74.81; H, 5.93; N, 2.61
2a (81)	−26.0	8.15	7.77–7.19	5.06	3.62 (8.0)	1.19	-	-
2b (89)	−26.0	7.83	7.60–7.21	5.07	3.69 (3.6)	1.63	-	-
2c (88)	−26.5 ^c	9.34 (8.17)	7.71–7.19	5.27	3.61 (4.8)	1.63	-	-
2d (65)	−27.1	9.05 (8.68)	7.55–7.32, 6.95, 6.61, 6.41	3.69	3.81 (4.8)	2.04	3047 (3228)	Calc. for C ₃₅ H ₃₄ N ₂ O ₂ P ₂ , C, 72.91; H, 5.94; N, 4.86 Found, C, 72.72; H, 5.95; N, 4.88
2e (80)	−27.1	9.29 (9.08)	7.46–7.35, 7.29, 6.86, 6.15	3.73	3.82 (4.4)	2.08	3178 (3317)	Calc. for C ₃₅ H ₃₄ N ₂ O ₂ P ₂ , C, 72.91; H, 5.94; N, 4.86 Found, C, 72.71; H, 5.94; N, 4.82
2f (70)	−27.5	9.31 (9.07)	7.41–7.03, 6.94, 6.40, 6.30	3.69	3.77 (4.4)		3163 (3283)	Calc. for C ₃₄ H ₃₂ N ₂ O ₂ P ₂ , C, 72.59; H, 5.73; N, 4.98 Found, C, 72.10; H, 5.80; N, 4.95
2g (85)	−26.8	9.09 (8.78)	7.36–7.25, 6.83, 6.53	3.61	3.72 (4.4)		3300 (3257)	Calc. for C ₃₄ H ₃₂ N ₂ O ₂ P ₂ , C, 72.59; H, 5.73; N, 4.98 Found, C, 72.15; H, 5.72; N, 4.95
3 (53)	−27.6	9.12	7.38–7.31, 6.92, 6.30, 6.13		3.85		3376	Calc. for C ₃₂ H ₂₉ NOP ₂ , C, 76.03; H, 5.78; N, 2.77 Found, C, 75.67; H, 5.71; N, 2.74

^a Isolated yields in parentheses. ^b Recorded in (CD₃)₂SO unless otherwise stated. ^c Recorded in CDCl₃. ^d $^2J(\text{PH})$ coupling in brackets.

^e Recorded as KBr discs.

The synthesis of ditertiary phosphines, containing a flexible backbone presenting extra donor/acceptor sites with additional H-bonding capability, is described here with the opportunity to enhance solid-state packing behaviour. The precursors for the synthesis of the desired functionalised ditertiary phosphines **2a–g** were prepared using, in step (i), 1 equiv. of primary amine, *N*-carbonyloxyglycine (1 equiv.) and dicyclohexylcarbodi-

imide (DCC, 1 equiv.) in THF affording the corresponding carbamates followed by, in step (ii), treatment with Pd/C and cyclohexene in C₂H₅OH, to give the desired primary alkylamines in moderate to good yields [30,31]. Using a similar procedure to that described for **1a–e**, the amide-functionalised diphosphines **2a–e** were prepared in 65–89% yields by condensation using 1 equiv. of primary amine and two equiv. of Ph₂PCH₂OH at r.t. in CH₃OH (Scheme 1). Furthermore, the phenol-substituted phosphines **2f** and **2g** were synthesised to investigate what effect, if any, an absent methyl group on the N-arene ring displays. In the case of **2d–g**, the diphosphines were obtained as solids whereas **2a–c** were obtained as yellow oils that were sufficiently pure to be used in complexation studies. All compounds displayed a single ³¹P NMR resonance around δ(P) –26 ppm [12–15,29] indicating the inclusion of an amide spacer has negligible effect on the ³¹P chemical shift. Other spectroscopic and analytical data are given in Table 1.

2.2. Single Crystal X-ray Studies of **1a**, **1b**·CH₃OH, **2f**·CH₃OH, **2g**, and **3**

X-ray quality crystals of **1a**, **1b**·CH₃OH, **2f**·CH₃OH, **2g**, and **3** were obtained by slow evaporation of a methanol solution, while for **2g** diethyl ether was diffused into a deuteriochloroform/methanol solution (Table 2).

Table 2. Details of the X-ray data collections and refinements for compounds **1a**, **1b**·CH₃OH, **2f**·CH₃OH, **2g**, and **3**.

Compound	1a	1b ·CH ₃ OH	2f ·CH ₃ OH	2g	3
Formula	C ₃₃ H ₃₁ NOP ₂	C ₃₄ H ₃₅ NO ₂ P ₂	C ₃₅ H ₃₆ N ₂ O ₃ P ₂	C ₃₄ H ₃₂ N ₂ O ₂ P ₂	C ₃₂ H ₂₉ NOP ₂
<i>M</i>	519.53	551.57	594.60	562.55	505.50
Crystal dimensions	0.42 × 0.15 × 0.03	0.13 × 0.12 × 0.02	0.24 × 0.18 × 0.16	0.25 × 0.18 × 0.15	0.31 × 0.28 × 0.03
Crystal morphology and colour	Plate, colourless	Block, colourless	Block, colourless	Block, colourless	Plate, colourless
Crystal system	Monoclinic	Monoclinic	Triclinic	Monoclinic	Triclinic
Space group	<i>P</i> 2 ₁ / <i>n</i>	<i>P</i> 2 ₁ / <i>c</i>	<i>P</i> $\bar{1}$	<i>I</i> a	<i>P</i> $\bar{1}$
<i>a</i> /Å	17.367(5)	10.3050(3)	12.6198(3)	11.6234(10)	10.5860(4)
<i>b</i> /Å	8.522(2)	32.8017(10)	16.2027(4)	21.7359(19)	10.7397(4)
<i>c</i> /Å	20.382(6)	8.5189(2)	17.8529(4)	11.6340(10)	13.4172(6)
α/°			64.0678(10)		73.1667(6)
β/°	114.673(4)	92.7318(16)	76.7403(14)	93.8717(14)	80.4518(7)
γ/°			75.5070(14)		63.1422(6)
<i>V</i> /Å ³	2741.2(13)	2876.30(14)	3148.15(13)	2932.6(4)	1301.45(9)
<i>Z</i>	4	4	4	4	2
λ/Å	0.71073	0.71073	0.71073	0.71073	0.71073
<i>T</i> /K	150(2)	120(2)	120(2)	150(2)	150(2)
Density (calcd.)/Mg/m ³	1.259	1.274	1.255	1.274	1.290
μ/mm ^{−1}	0.185	0.183	0.176	0.182	0.193
θ range/°	2.02–26.60	3.03–27.53	3.24–25.00	1.87–28.82	1.59–30.62
Measured reflections	23,525	27,247	61,330	12,577	15,576
Independent reflections	5708	6545	11,047	6586	7814
Observed reflections (<i>F</i> ² > 2σ(<i>F</i> ²))	3115	5019	7559	5293	6116
<i>R</i> _{int}	0.124	0.058	0.095	0.039	0.027
<i>R</i> [<i>F</i> ² > 2σ(<i>F</i> ²)] ^a	0.0743	0.0799	0.0517	0.0389	0.0441
<i>wR</i> 2 [all data] ^b	0.2205	0.1650	0.1220	0.0861	0.1248
Largest difference map features/eÅ ^{−3}	1.40, −0.49	0.46, −0.52	0.38, −0.30	0.29, −0.16	0.51, −0.21

^a $R = \sum ||F_o| - |F_c|| / \sum |F_o|$. ^b $wR2 = [\sum [w(F_o^2 - F_c^2)^2] / \sum [w(F_o^2)^2]]^{1/2}$.

The geometry around each phosphorus atom is essentially pyramidal as would be anticipated (Figures 1–5). The P^{III} atoms are in an *anti* conformation, presumably to minimise steric repulsions between the phenyl groups. The geometry about the N(1) centre is approx. pyramidal [$\Sigma(\text{C}-\text{N}(1)-\text{C})$ angles: $337.0(3)^\circ$ for **1a**; $335(2)^\circ$ for **1b**·CH₃OH; $335.2(2)/336.6(2)^\circ$ for **2f**·CH₃OH; $333.7(2)^\circ$ for **2g**] and approximately trigonal planar for **3** [$\Sigma(\text{C}-\text{N}-\text{C}) = 359.05(11)^\circ$]. In **1a** and **1b**·CH₃OH, the N-arene ring [C(3) > C(8)] is twisted by ca. 88° (**1a**) and 86° (**1b**·CH₃OH) [12,32] such that it is almost perpendicular to the C(1)–N(1)–C(2) plane, whereas for **3**, the twist of the C(1)–N(1)–C(2) fragment is around 9° from co-planarity with the N-arene group, apparently as a result of the intermolecular H-bonding requirements (*vide infra*).

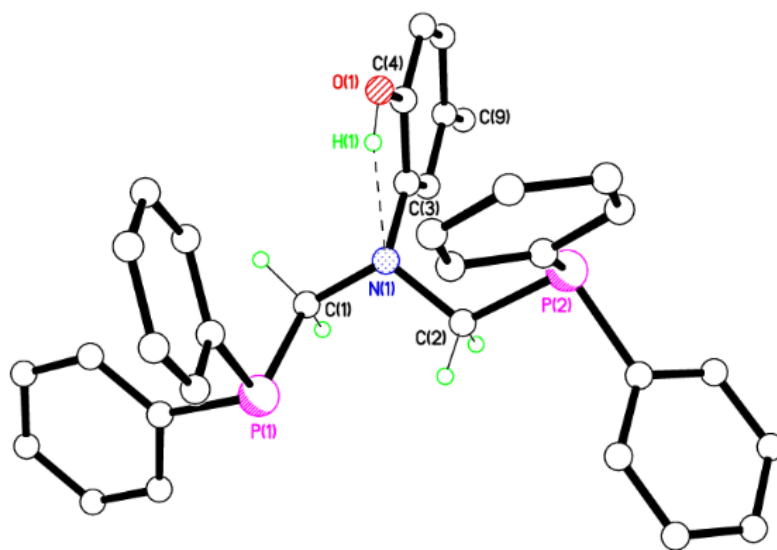


Figure 1. Molecular structure of **1a**. All hydrogens, except on C(1), C(2) and O(1), have been omitted for clarity.

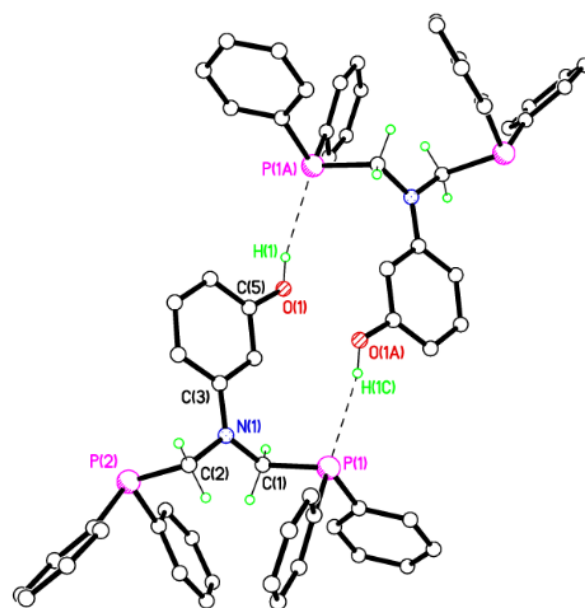


Figure 2. Molecular structure of **3** showing a dimer pair. All hydrogens, except on C(1), C(2) and O(1), have been omitted for clarity. Symmetry code: A = $1 - x, 1 - y, 1 - z$.

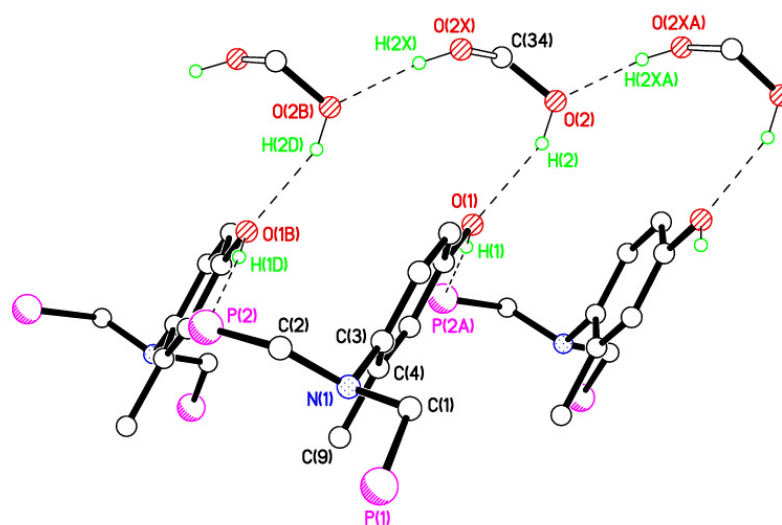


Figure 3. Crystal structure packing plot for **1b**·CH₃OH. Most H atoms, two Ph groups per P atom have been omitted for clarity. Symmetry code: A = $x, -y + \frac{1}{2}, z + \frac{1}{2}$.

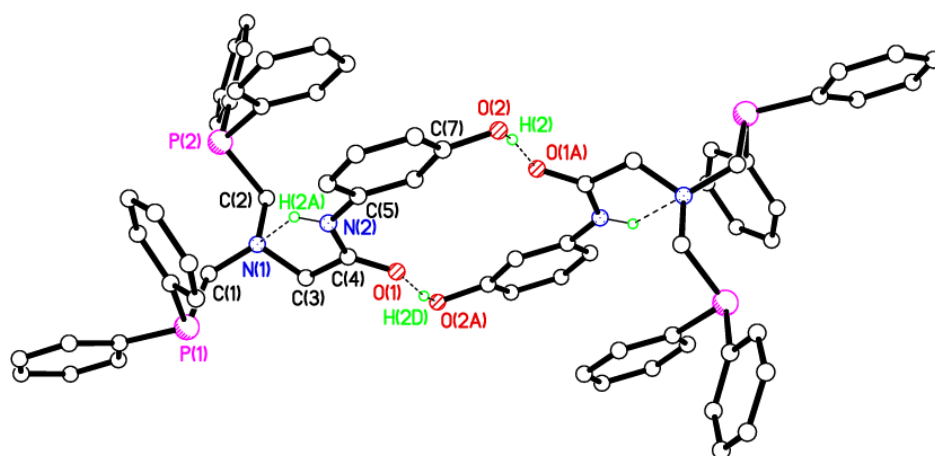


Figure 4. Dimers of **2f** forming $R^2_2(16)$ graph set motifs. Most H atoms omitted for clarity. The second unique molecule which adopts a similar, centrosymmetric motif, is not shown.

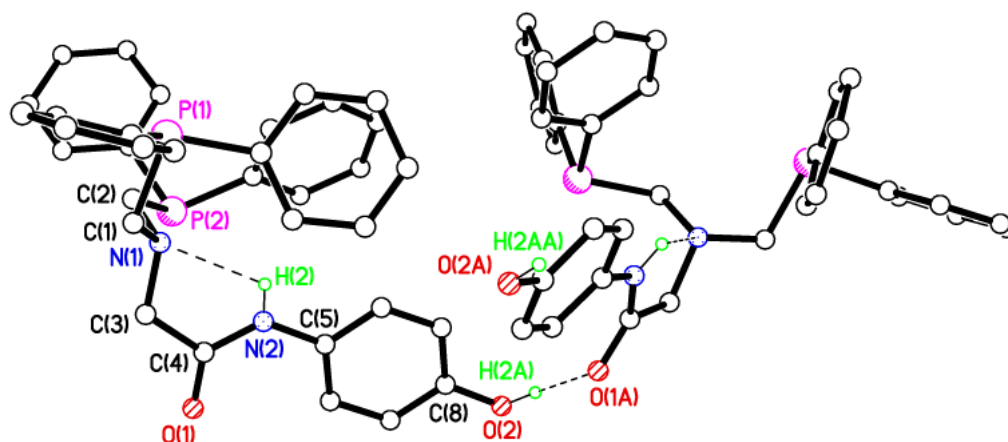


Figure 5. Intra- and intermolecular interactions in the crystal structure of **2g**. Most H atoms omitted for clarity. Symmetry operator A = $x, -y + \frac{3}{2}, z - \frac{1}{2}$.

2.3. Secondary Interactions in **1a**, **1b**·CH₃OH, **2f**·CH₃OH, **2g**, and **3**

The synthons observed in the solid state for these highly modular ligands may be dictated by various factors including the nature of the ligand, the flexibility of the P–C–N–C–P backbone, the predisposition of the OH/CH₃ groups about the N-arene ring, and the solvent used in the crystallisation. In order to probe the OH/CH₃ interplay of groups, the crystal structure of **1a**, with the –OH group in the *ortho* position with respect to the N(1) atom, is described first. Ligand **1a** crystallises with an intramolecular S(5) [33–35] H-bonded ring with $d = 2.26(5)$ Å [denoting the hydrogen (H) to acceptor (A) distance in an H-bond D–H···A] [36] for the O–H···N interaction (Figure 1). The intramolecular H-bonding in **1a** limits the dimensionality of the packing of the diphosphine ligand. Therefore, the structure of **1a** is essentially zero-dimensional (Table 3).

Table 3. Selected data ($D\cdots A/\text{Å}$, $\angle D\cdots H\cdots A/^\circ$) for key inter- and intramolecular contacts for compounds **1a**, **1b**·CH₃OH, **2f**·CH₃OH, **2g**, and **3**.

	1a	1b ·CH ₃ OH	2f ·CH ₃ OH ^a	2g	3
O–H···N _{intra}	2.745(4), 119(4)				
O–H _{MeOH} ···O _{inter}		2.844(8), 157			
O–H _{MeOH} ···O _{MeOH}		2.781(11), 172			
O–H···P _{inter}		3.432(3), 173			3.4400(12), 167(2)
O–H···(O) _{Cinter}			2.671(3), 171(3) [2.659(3), 165(3)]	2.706(4), 169(4)	
N–H···N _{intra}			2.695(3), 114(2) [2.714(3), 117(2)]	2.748(4), 114(3)	

^a Values in parentheses are for the second independent molecule.

Compound **3**, where the –OH functional group is in the *meta* position with respect to the tertiary N(1) atom, aggregates in the solid state in such a way that fairly weak hydrogen bonds, O–H···P [$d = 2.60(2)$ Å], form between symmetry-related molecules, creating dimers in which two ligands are held in an $R^2_2(16)$ H-bonding motif (Figure 2). The distance between symmetry-related nitrogen atoms is 8.257 Å. The structure of **3** shows a 0D arrangement.

Compound **1b**·CH₃OH, which contains the –OH group in a *para* position with respect to the N-arene, displays a similar structure to **3** with intramolecular O–H···P interactions at $d = 2.60$ Å. However, instead of forming dimers, there are 1D zig-zag chains in the *c* direction (Figure 3). The *para* hydroxyl oxygen acts as an acceptor for an O–H···O intermolecular H-bond from approximately alternate CH₃OH molecules of crystallisation with $d = 2.05$ Å. These CH₃OH molecules are 50/50 disordered with the second component H-bonding to its neighbour with $d = 1.95$ Å. Selected hydrogen parameters for **1b**·CH₃OH are listed in Table 3.

Compound **2f**·CH₃OH crystallises with two, similarly behaved, molecules in the asymmetric unit. A pair of H-bonded molecules, related by inversion symmetry, and with $d = 1.81(3)$ Å for the intermolecular O–H···O interaction [1.78(3) Å for molecule 2] affords $R^2_2(16)$ ring motifs (Figure 4). The intramolecular N–H···N S(5) H-bond motif with $d = 2.25(3)$ Å [2.26(3) Å for molecule 2] results in an intermediate twist angle of 64.23(13)° [but a rather more perpendicular 78.70(8)° for molecule 2] between planes C(1)/N(1)/C(2) and ring C(5) > C(10) [plane C(35)/N(4)/C(36) and ring C(39) > C(44) for molecule 2]. The *meta* hydroxy group in **2f** facilitates 0D dimer formation, as opposed to the chains observed in **2g** (*vide infra*).

For **2g**, molecules form H-bonded, 1D, zig-zag chains in the *c* direction via strong O–H···O interactions with $d = 1.83(5)$ Å (Figure 5). The intramolecular N–H···N S(5), H-bond motif with $d = 2.29(3)$ Å again results in an almost perpendicular twist angle of 82.09(15)° between planes C(1)/N(1)/C(2) and arene ring C(5) > C(10). The *para* hydroxy group promotes chain formation.

2.4. Dichloroplatinum(II) Complexes of 1a–e, 2a–g, and 3

The synthesis of *P,P*-chelate complexes *cis*-PtCl₂(1a–e) [4a–e], *cis*-PtCl₂(2a–g) [5a–g], and *cis*-PtCl₂(3) [6] (Chart 2) was achieved by stirring the ligands and PtCl₂(η⁴-cod) (1:1 ratio) in CH₂Cl₂ for 1.5 h with displacement of the cod ligand. The products were isolated in good yields as colourless solids. Downfield shifts of the ³¹P NMR resonances were observed for all complexes, with ¹J_{PtP} coupling constants of approx. 3400 Hz, indicative of a *cis* conformation [29]. This was further supported by two characteristic ν_{PtCl} IR vibrations in the range of 279–316 cm^{−1} (Table 4). Furthermore, compounds 4a–e, 5a–g, and 6 present ν(NH) and ν(OH) IR absorptions in the range 3050–3465 cm^{−1} and also a strong band in the region of 1653–1675 cm^{−1}, indicative of ν(C=O amide).

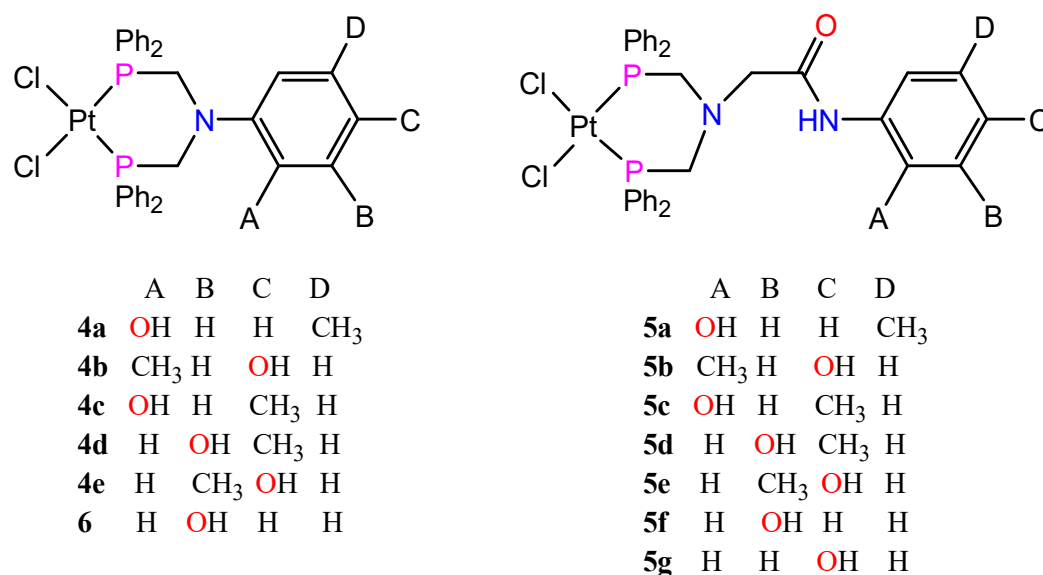


Chart 2. Structures of compounds 4a–e, 5a–g, and 6.

Table 4. Selected spectroscopic and analytical data for compounds 4a–6^a.

Compound ^a	δ(P) ^b	δ(H) /OH (NH)	δ(H) /arom. H.	δ(H) /CH ₂	δ(H) /CH ₂	δ(H) /CH ₃	ν _f ^{OH} (ν _{NH})	ν _{PtCl}	Microanalysis (CHN)
4a (98)	−9.4 ^d (3424)	9.25	7.89–7.80, 7.64–7.46, 6.68, 5.90		4.21	1.93	3314	316, 289	Calc. for C ₃₃ H ₃₁ Cl ₂ NOP ₂ Pt·CH ₂ Cl ₂ , C, 46.91; H, 3.82; N, 1.61 Found, C, 47.07; H, 3.77; N, 1.69
4b (89)	−4.9 ^d (3426)	9.22	7.96–7.53, 6.96, 6.49, 6.33		4.19	1.29	3373	315, 282	Calc. for C ₃₃ H ₃₁ Cl ₂ NOP ₂ Pt, C, 50.46; H, 3.98; N, 1.78 Found, C, 50.51; H, 4.13; N, 1.83
4c (78)	−8.6 ^d (3436)	9.42	7.89–7.84, 7.56–7.43, 6.59, 6.30, 6.05		4.16	2.06	3433	309, 290	Calc. for C ₃₃ H ₃₁ Cl ₂ NOP ₂ Pt·0.5CH ₂ Cl ₂ , C, 48.96; H, 3.87; N, 1.68 Found, C, 49.42; H, 3.96; N, 1.73
4d (98)	−11.7 ^d (3410)	8.44	7.94–7.87, 7.78–7.62, 6.86, 6.47		4.43	2.02	3421	314, 290	Calc. for C ₃₃ H ₃₁ Cl ₂ NOP ₂ Pt, C, 50.46; H, 3.98; N, 1.78 Found, C, 50.24; H, 3.98; N, 1.85
4e (81)	−7.8 ^d (3421)	9.01	7.96–7.85, 7.59–7.45, 6.75, 6.27, 6.03		4.33	2.09	3416	316, 284	Calc. for C ₃₃ H ₃₁ Cl ₂ NOP ₂ Pt, C, 50.46; H, 3.98; N, 1.78 Found, C, 50.66; H, 4.61; N, 1.70

Table 4. Cont.

Compound ^a	$\delta(P)$ ^b	$\delta(H)$ /OH (NH)	$\delta(H)$ /arom. H.	$\delta(H)$ /CH ₂	$\delta(H)$ /CH ₂	$\delta(H)$ /CH ₃	ν_{OH} (ν_{NH}) _f	ν_{PtCl}	Microanalysis (CHN)
5a (89)	−9.8 ^{d,e} (3398)	9.45 (8.91)	7.84–7.80, 7.53–7.44, 6.69	3.49	4.05	2.22	3051 (3249)	305, 283	Calc. for C ₃₅ H ₃₄ Cl ₂ N ₂ O ₂ P ₂ Pt·0.5CH ₂ Cl ₂ , C, 48.63; H, 3.74; N, 3.15 Found, C, 49.00; H, 4.07; N, 3.13
5b (65)	−11.0 ^d (3397)	9.16 (8.61)	7.83–7.80, 7.57–7.41, 7.05, 6.48	4.03	4.03	1.80	3050 (3350)	316, 283	Calc. for C ₃₅ H ₃₄ Cl ₂ N ₂ O ₂ P ₂ Pt, C, 49.89; H, 4.07; N, 3.32 Found, C, 49.32; H, 4.17; N, 3.25
5c (73)	−9.9 ^d (3405)	9.56 (8.94)	7.85–7.77, 7.59–7.38, 6.63, 6.51	3.17	4.05	2.17	3075 (3347)	315, 290	Calc. for C ₃₅ H ₃₄ Cl ₂ N ₂ O ₂ P ₂ Pt, C, 49.89; H, 4.07; N, 3.32 Found, C, 49.28; H, 4.05; N, 2.91
5d (99)	−9.8 ^{c,d} (3406)	9.17 (8.90)	7.98–7.50, 6.97–6.84, 6.68, 6.73	3.20	4.66	2.13	3323 (3465)	309, 283	Calc. for C ₃₅ H ₃₄ Cl ₂ N ₂ O ₂ P ₂ Pt·0.5C ₄ H ₁₀ O, C, 50.52; H, 4.47; N, 3.19 Found, C, 50.91; H, 4.53; N, 3.61
5e (90)	−9.7 ^{c,d} (3406)	9.46 (9.21)	7.94–7.78, 7.54–7.42, 7.09, 6.87, 6.69	3.43	4.12	2.02	3287 (3439)	312, 286	Calc. for C ₃₅ H ₃₄ Cl ₂ N ₂ O ₂ P ₂ Pt, C, 49.89; H, 4.07; N, 3.32 Found, C, 49.77; H, 3.95; N, 3.38
5f (85)	−9.5 ^{c,d} (3425)	9.62 (9.36)	7.91–7.86, 7.60–7.42, 7.05, 6.83, 6.45	3.47	4.18		3053 (3312)	304, 279	Calc. for C ₃₄ H ₃₂ Cl ₂ N ₂ O ₂ P ₂ Pt, C, 49.29; H, 3.89; N, 3.38 Found, C, 48.98; H, 3.38; N, 3.37
5g (84)	−9.5 ^{c,d} (3405)	9.52 (9.31)	8.01–7.97, 7.70–7.61, 7.34, 6.78	3.49	4.26		3054 (3325)	311, 287	Calc. for C ₃₄ H ₃₂ Cl ₂ N ₂ O ₂ P ₂ Pt, C, 49.29; H, 3.89; N, 3.38 Found, C, 48.72; H, 3.66; N, 3.33
6 (89)	−4.0 ^d (3436)	8.45	7.45–7.05, 6.89–6.76, 6.31,		4.31		3356	311, 289	Calc. for C ₃₂ H ₂₉ Cl ₂ NOP ₂ Pt, C, 49.82; H, 3.79; N, 1.82 Found, C, 49.31; H, 3.58; N, 1.79

^a Isolated yields in parentheses. ^b Recorded in (CD₃)₂SO unless otherwise stated. ^c Recorded in CDCl₃. ^d ¹J(PtP) coupling in parentheses. ^e Recorded in CDCl₃/CD₃OD. ^f Recorded as KBr discs.

2.5. Single Crystal X-ray Studies of Complexes **4b**·(CH₃)₂SO, **4c**·CHCl₃, **4d**· $\frac{1}{2}$ Et₂O, **4e**· $\frac{1}{2}$ CHCl₃· $\frac{1}{2}$ CH₃OH, **5a**· $\frac{1}{2}$ Et₂O, **5b**, **5c**· $\frac{1}{4}$ H₂O, **5d**·Et₂O, and **6**·(CH₃)₂SO

Detailed single crystal X-ray analysis (Tables 5 and 6) of complexes **4b**·(CH₃)₂SO, **4c**·CHCl₃, **4d**· $\frac{1}{2}$ Et₂O, **4e**· $\frac{1}{2}$ CHCl₃· $\frac{1}{2}$ CH₃OH, **5a**· $\frac{1}{2}$ Et₂O, **5b**, **5c**· $\frac{1}{4}$ H₂O, **5d**·Et₂O, and **6**·(CH₃)₂SO shows that the geometry about each Pt(II) centre is approximately square planar [P–Pt–P range 90.23(9)–96.52(3)°] (Tables 7 and 8). The Pt–Cl and Pt–P bond distances are consistent with literature values [29] and the conformation of the Pt–P–C–N–C–P six-membered ring in each complex is best described as a boat. The dihedral angle measured between the P₂C₂ plane and N-arene ring least-squares planes varies between 50.98(12)° [in **6**·(CH₃)₂SO] and 90° (in **5d**·Et₂O), the difference of ca. 39° may tentatively be explained by the predisposition of the –OH group about the N-arene group and subsequent H-bonding requirements. Upon metal chelation, a degree of freedom, compared with the free ligands **1a**, **1b**·CH₃OH, **2f**·CH₃OH, **2g**, and **3** has been removed, as the P–C–N–C–P backbone is locked into a specific conformation. Unfortunately, we were unable to obtain suitable X-ray quality crystals of compounds **4a** and **5e–g**.

Table 5. Details of the X-ray data collections and refinements for compounds **4b**·(CH₃)₂SO, **4c**·CHCl₃, **4d**·½OEt₂, and **4e**·½CHCl₃·½CH₃OH.

Compound	4b ·(CH ₃) ₂ SO	4c ·CHCl ₃	4d ·½OEt ₂	4e ·½CHCl ₃ ·½CH ₃ OH
Formula	C ₃₅ H ₃₇ Cl ₂ N ₂ O ₂ P ₂ PtS	C ₃₄ H ₃₂ Cl ₅ N ₂ O ₂ Pt	C ₃₅ H ₃₆ Cl ₂ N ₂ O _{1.5} P ₂ Pt	C ₃₄ H _{33.5} Cl _{3.5} N ₂ O _{1.5} P ₂ Pt
<i>M</i>	863.64	904.88	822.58	861.22
Crystal dimensions	0.19 × 0.02 × 0.01	0.30 × 0.18 × 0.04	0.13 × 0.06 × 0.03	0.15 × 0.04 × 0.02
Crystal morphology and colour	Needle, colourless	Plate, colourless	Lath, colourless	Needle, colourless
Crystal system	Tetragonal	Monoclinic	Monoclinic	Monoclinic
Space group	<i>P</i> 4 ₃	<i>P</i> 2 ₁ / <i>n</i>	<i>P</i> 2 ₁ / <i>c</i>	<i>P</i> 2 ₁ / <i>n</i>
<i>a</i> /Å	11.373(3)	11.6938(4)	15.7344(6)	21.4521(4)
<i>b</i> /Å		16.7052(6)	17.0714(6)	12.5164(2)
<i>c</i> /Å	26.773(6)	18.2242(7)	13.9632(5)	24.5837(4)
α/°				
β/°		99.7066(6)	92.0800(4)	92.2343(5)
γ/°				
<i>V</i> /Å ³	3463(2)	3509.1(2)	3748.2(2)	6595.78(19)
<i>Z</i>	4	4	4	8
λ/Å	0.71073	0.71073	0.6710	0.71073
<i>T</i> /K	150(2)	150(2)	150(2)	120(2)
Density (calcd.)/Mg/m ³	1.657	1.713	1.458	1.735
μ/mm ⁻¹	4.391	4.500	3.425	4.666
θ range/°	1.79–26.09	1.67–31.09	1.78–31.10	2.94–27.49
Measured reflections	29,848	32,600	48,268	84,353
Independent reflections	6852	10,997	13,239	15,063
Observed reflections (<i>F</i> ² > 2σ(<i>F</i> ²))	5560	8926	10,918	12,905
<i>R</i> _{int}	0.110	0.043	0.039	0.049
<i>R</i> [<i>F</i> ² > 2σ(<i>F</i> ²)] ^a	0.0473	0.0303	0.0266	0.0561
<i>wR</i> 2 [all data] ^b	0.1015	0.0660	0.0646	0.1202
Largest difference map features/eÅ ⁻³	1.43, −0.91	1.29, −1.08	0.84, −0.67	1.64, −1.48

$$^a R = \sum ||F_o| - |F_c|| / \sum |F_o|. \quad ^b wR2 = [\sum [w(F_o^2 - F_c^2)^2] / \sum [w(F_o^2)^2]]^{1/2}.$$

Table 6. Details of the X-ray data collections and refinements for compounds **5a**·½OEt₂, **5b**, **5c**·¼H₂O, **5d**·OEt₂, and **6**·(CH₃)₂SO.

Compound	5a ·½OEt ₂	5b	5c ·¼H ₂ O	5d ·OEt ₂	6 ·(CH ₃) ₂ SO
Formula	C ₃₇ H ₃₉ Cl ₂ N ₂ O _{2.5} P ₂ Pt	C ₃₅ H ₃₄ Cl ₂ N ₂ O ₂ P ₂ Pt	C ₃₅ H _{34.5} Cl ₂ N ₂ O _{2.25} P ₂ Pt	C ₃₉ H ₄₄ Cl ₂ N ₂ O ₃ P ₂ Pt	C ₃₄ H ₃₅ Cl ₂ N ₂ O ₂ P ₂ PtS
<i>M</i>	879.63	842.57	842.57	916.69	849.62
Crystal dimensions	0.12 × 0.06 × 0.05	0.05 × 0.02 × 0.01	0.09 × 0.05 × 0.02	0.13 × 0.12 × 0.02	0.32 × 0.11 × 0.02
Crystal morphology and colour	Block, colourless	Plate, colourless	Plate, colourless	Plate, colourless	Needle, colourless
Crystal system	Trigonal	Monoclinic	Triclinic	Orthorhombic	Monoclinic
Space group	<i>P</i> 3 ₂	<i>P</i> 2 ₁ / <i>n</i>	<i>P</i> 1̄	<i>Pbcm</i>	<i>P</i> 2 ₁ / <i>n</i>
<i>a</i> /Å	24.3688(7)	18.2384(7)	8.4021(6)	10.125(6)	9.7763(4)
<i>b</i> /Å		8.1955(3)	10.3896(7)	19.790(11)	13.0930(5)
<i>c</i> /Å	10.6567(6)	23.5809(10)	21.8810(15)	18.407(10)	25.8715(10)
α/°			92.8380(10)		
β/°		111.4543(5)	97.9841(9)		95.1690(6)
γ/°			106.6253(8)		
<i>V</i> /Å ³	5480.5(4)	3280.5(2)	1804.5(2)	3688(4)	3298.1(2)
<i>Z</i>	6	4	2	4	4
λ/Å	0.7848	0.6910	0.6710	0.71073	0.71073
<i>T</i> /K	150(2)	120(2)	150(2)	150(2)	150(2)
Density (calcd.)/Mg/m ³	1.599	1.706	1.559	1.651	1.711
μ/mm ⁻¹	5.266	4.225	3.561	4.077	4.609
θ range/°	3.69–33.17	1.19–31.01	2.71–30.94	2.01–25.00	1.58–30.64
Measured reflections	48,822	37,553	22,910	25,092	38,887

Table 6. Cont.

Compound	5a·½OEt ₂	5b	5c·¼H ₂ O	5d·OEt ₂	6·(CH ₃) ₂ SO
Independent reflections	19,298	10,642	12,184	3357	10,104
Observed reflections ($F^2 > 2\sigma(F^2)$)	17,145	8283	10,104	2051	7753
R_{int}	0.071	0.063	0.053	0.1504	0.0572
$R[F^2 > 2\sigma(F^2)]^a$	0.0542	0.0363	0.0507	0.0746	0.0356
$wR2$ [all data] ^b	0.1551	0.0842	0.1341	0.2065	0.0816
Largest difference map features/eÅ ⁻³	1.59, -1.71	1.40, -1.47	2.34, -3.46	2.77, -1.91	1.97, -1.50

$$^a R = \sum ||F_o| - |F_c|| / \sum |F_o|. \quad ^b wR2 = [\sum [w(F_o^2 - F_c^2)^2] / \sum [w(F_o^2)^2]]^{1/2}.$$

Table 7. Selected bond distances and angles for dichloroplatinum(II) compounds 4b·(CH₃)₂SO, 4c·CHCl₃, 4d, and 4e·½CHCl₃·½CH₃OH.

Bond Length (Å)	4b·(CH ₃) ₂ SO	4c·CHCl ₃	4d	4e·½CHCl ₃ ·½MeOH ^a
Pt(1)–P(1)	2.223(4)	2.2226(6)	2.2257(6)	2.2386(18) [2.2353(18)]
Pt(1)–P(2)	2.225(4)	2.2186(7)	2.2146(6)	2.2475(18) [2.2464(18)]
Pt(1)–Cl(1)	2.358(4)	2.3625(6)	2.3558(6)	2.3560(18) [2.3574(17)]
Pt(1)–Cl(2)	2.359(4)	2.3484(6)	2.3553(6)	2.3694(17) [2.3616(18)]
Bond angle (°)				
Cl(1)–Pt(1)–P(1)	87.91(14)	86.12(2)	87.63(2)	87.30(7) [86.87(7)]
Cl(1)–Pt(1)–P(2)	174.97(15)	176.08(3)	175.93(2)	176.50(7) [176.84(7)]
Cl(1)–Pt(1)–Cl(2)	88.95(13)	88.68(2)	90.43(2)	88.13(7) [87.34(7)]
Cl(2)–Pt(1)–P(2)	86.71(13)	88.94(2)	85.53(2)	88.54(7) [90.04(7)]
Cl(2)–Pt(1)–P(1)	176.37(15)	174.73(2)	177.81(2)	169.14(7) [170.73(7)]
P(1)–Pt(1)–P(2)	96.35(14)	96.30(3)	96.42(2)	96.17(7) [95.95(7)]

^a Values in parentheses are for the second independent molecule.

Table 8. Selected bond distances and angles for dichloroplatinum(II) compounds 5a·½OEt₂, 5b, 5c·¼H₂O, 5d·OEt₂, and 6·(CH₃)₂SO.

Bond Length (Å)	5a·½OEt ₂ ^a	5b	5c·¼H ₂ O	5d·OEt ₂	6·(CH ₃) ₂ SO
Pt(1)–P(1)	2.233(3) [2.234(3)]	2.2172(9)	2.2268(12)	2.220(3)	2.2219(9)
Pt(1)–P(2)	2.230(3) [2.229(3)]	2.2249(9)	2.2196(12)	^c	2.2288(9)
Pt(1)–Cl(1)	2.381(3) [2.378(3)]	2.3685(9)	2.347(4) ^b	2.348(3)	2.3421(9)
Pt(1)–Cl(2)	2.361(3) [2.365(3)]	2.3425(9)	2.3638(12)	^c	2.3618(10)
Bond angle (°)					
Cl(1)–Pt(1)–P(1)	86.31(10) [86.48(10)]	85.73(3)	92.55(11)	89.98(12)	88.81(3)
Cl(1)–Pt(1)–P(2)	177.81(12) [177.51(12)]	176.29(3)	167.1(2)	176.96(13)	173.98(3)
Cl(1)–Pt(1)–Cl(2)	90.20(13) [90.16(13)]	89.33(3)	88.17(11)	87.38(17)	88.78(4)
Cl(2)–Pt(1)–P(2)	87.75(14) [87.51(13)]	88.31(3)	87.76(4)	89.98(12)	87.17(3)
Cl(2)–Pt(1)–P(1)	175.76(12) [175.67(12)]	174.72(3)	178.70(5)	176.96(13)	174.52(4)
P(1)–Pt(1)–P(2)	90.20(13) [95.81(11)]	96.52(3)	91.30(4)	92.62(17)	94.83(3)

^a Values in parentheses are for the second independent molecule. ^b 2-fold disorder. ^c Molecule lies on a mirror plane.

Despite the *ortho* position of the hydroxy group in 4c·CHCl₃, molecules do not form an intramolecular S(5) O–H···N interaction as seen in 1a (Figure 1), instead forming a bifurcated H-bond with the two coordinated chloride ligands of an adjacent molecule (Figure 6). This generates a 1D chain, and also attracts a bifurcated H-bonded chloroform

molecule. There are somewhat asymmetric distances d for H(1C) to Cl(1) and Cl(2) are 2.45(4) and 2.76(4) Å, while those from H(34) to Cl(1) and Cl(2) are 2.66 and 2.86 Å, so are also asymmetric. The twist angle between planes P(1)/P(2)/C(1)/C(2) and ring C(3) > C(8) is 84.83(8)°, so is almost perpendicular. Atoms N(1) and Pt(1) lie 0.795(4) and 0.024(2) Å away from the P(1)/P(2)/C(1)/C(2) plane, respectively. The hinge angle across the P(1)–P(2) vector is 2.51(5)°. Selected hydrogen bonding geometric parameters for 4c·CHCl₃ are shown in Table 9.

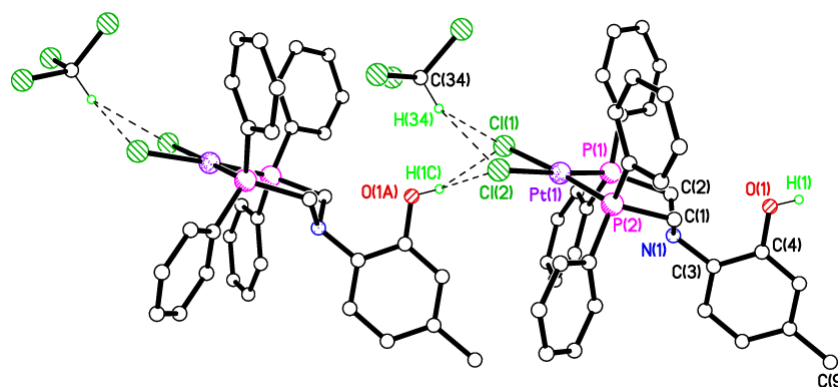


Figure 6. H-bonded packing arrangement in the crystal structure of 4c·CHCl₃. Most H atoms omitted for clarity. Symmetry operator A = $x + \frac{1}{2}, -y + \frac{1}{2}, z + \frac{1}{2}$.

Table 9. Selected data ($D \cdots A/\text{Å}$, $\angle D-H \cdots A/^\circ$) for key inter- and intramolecular contacts for compounds 4b·(CH₃)₂SO, 4c·CHCl₃, 4e· $\frac{1}{2}$ CHCl₃· $\frac{1}{2}$ CH₃OH, 5a· $\frac{1}{2}$ OEt₂, 5b, 5c· $\frac{1}{4}$ H₂O, 5d·OEt₂, and 6·(CH₃)₂SO.

	4b·(CH ₃) ₂ SO	4c·CHCl ₃	4e· $\frac{1}{2}$ CHCl ₃ · $\frac{1}{2}$ CH ₃ OH	5a· $\frac{1}{2}$ OEt ₂ ^a	5b	5c· $\frac{1}{4}$ H ₂ O	5d·OEt ₂	6·(CH ₃) ₂ SO
O–H \cdots (O) _{Cinter}						3.714(14), 169		
N–H \cdots N _{intra}					2.711(5), 107(4)	2.776(12), 108 ^b		
O–H _{inter} \cdots O _{MeOH}			2.624(10), 160					
O–H _{inter} \cdots Cl _{Pt}		3.145(2), 145(3) 3.361(2), 133(3)	3.197(6), 160(9)		3.065(3), 161(5)			
O–H _{inter} \cdots O _{(CH₃)₂SO}	2.716(17), 170							1.79(2), 173(5)
N–H _{inter} \cdots Cl _{Pt}				3.328(12), 145(16) 3.320(11), 159(16) 2.596(13), 157			3.505(15), 138(6)	
O–H \cdots (O) _{Cintra}				2.610(13), 175(20)				

^a Values in parentheses are for the second independent molecule. ^b For the major disorder component; 2.658(12), 117 for the minor component.

Compound 6·(CH₃)₂SO, in which the –OH group is *meta* to the N-arene group H-bonds to the DMSO molecule of crystallisation resulting in a 0D structure (Figure 7). The distance d for this H-bond is 1.79(2) Å. The twist angle between plane P(1)/P(2)/C(1)/C(2) and ring C(3) > C(8) is 50.98(12)°. Atoms N(1) and Pt(1) lie 0.758(4) and 0.404(2) Å away from the P(1)/P(2)/C(1)/C(2) plane, respectively, so is more chair-shaped than some of the

other platinum(II) complexes reported here. The hinge angle across the P(1)–P(2) vector is $11.87(13)^\circ$.

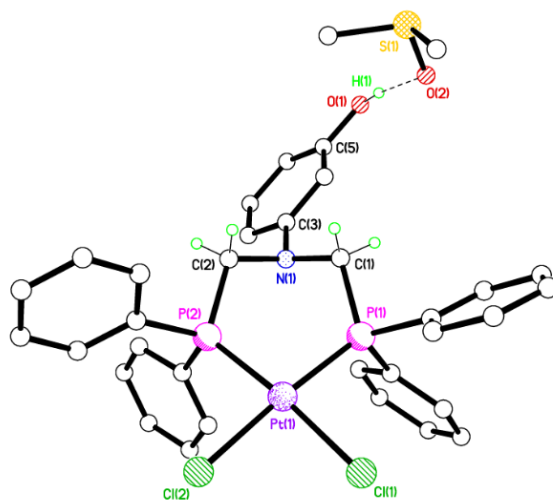


Figure 7. Crystal structure of $6 \cdot (\text{CH}_3)_2\text{SO}$ showing the hydroxyl group H-bonding to the $(\text{CH}_3)_2\text{SO}$ molecule of crystallisation. Most H-atoms omitted for clarity.

For $4\mathbf{d} \cdot \frac{1}{2}\text{Et}_2\text{O}$ (Figure 8) a molecule of badly disordered diethyl ether, modelled by the Platon Squeeze procedure, is not shown, but is in the vicinity of the hydroxy group and may H-bond to it resulting in a 0D structure. The twist angle between plane P(1)/P(2)/C(1)/C(2) and ring C(3) > C(8) is $67.82(7)^\circ$. Atoms N(1) and Pt(1) lie $0.797(3)$ and $0.2378(16)$ Å away from the P(1)/P(2)/C(1)/C(2) plane, respectively. The hinge angle across the P(1)–P(2) vector is $9.20(9)^\circ$.

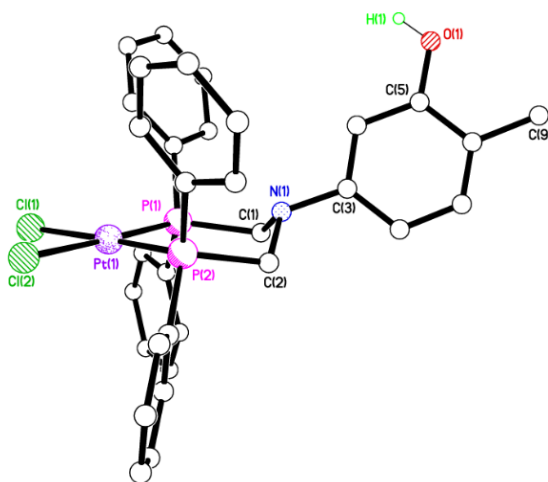


Figure 8. Crystal structure of $4\mathbf{d} \cdot \frac{1}{2}\text{Et}_2\text{O}$. Most H atoms and the disordered OEt_2 molecule omitted for clarity.

The crystal structure of $4\mathbf{b} \cdot (\text{CH}_3)_2\text{SO}$ shows the hydroxy group H-bonding to the DMSO molecule of crystallisation (Figure 9a). The distance d for this H-bond is 1.89 Å. The twist angle between plane P(1)/P(2)/C(1)/C(2) and ring C(3) > C(8) is $72.2(4)^\circ$. Atoms N(1) and Pt(1) lie $0.781(17)$ and $0.180(10)$ Å away from the P(1)/P(2)/C(1)/C(2) plane, respectively. The hinge angle across the P(1)–P(2) vector is $8.7(6)^\circ$. Molecules form 1D, weakly H-bonded, undulating chains in the c direction via the methylene H atoms on C(1) and C(2) to a single, coordinated chloride ligand in an adjacent molecule (Figure 9b). Selected hydrogen bonding parameters for $4\mathbf{b} \cdot (\text{CH}_3)_2\text{SO}$ are shown in Table 9.

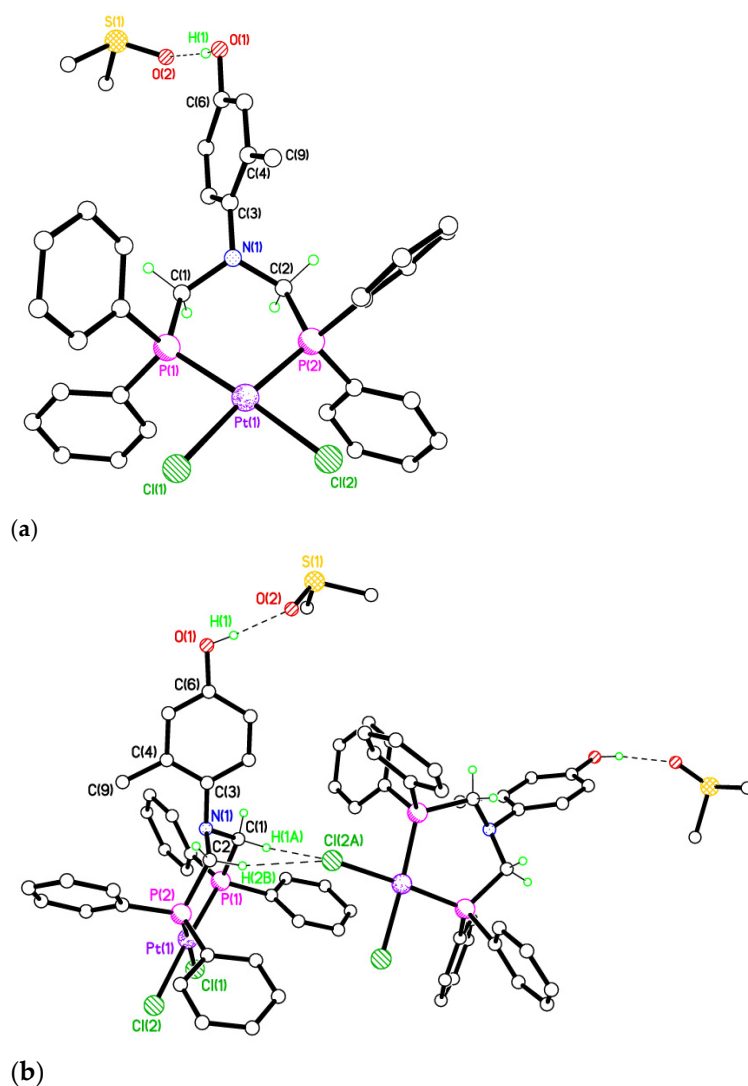


Figure 9. (a) Crystal structure of $4b \cdot (\text{CH}_3)_2\text{SO}$ showing the hydroxyl group H-bonding to the DMSO molecule of crystallisation. Most H-atoms removed for clarity. (b) Packing interactions in the crystal structure of $4b \cdot (\text{CH}_3)_2\text{SO}$. Most H atoms omitted for clarity. Symmetry operator $A = y - 1, 1 - x, \frac{1}{4} + z$.

For compound $4e \cdot \frac{1}{2}\text{CHCl}_3 \cdot \frac{1}{2}\text{CH}_3\text{OH}$ there are two independent Pt complexes, one CH_3OH , and one CHCl_3 in the asymmetric unit. Both Pt complexes form 1D chains aligned parallel to b , but these chains are different (Figure 10). The chain involving Pt(2) forms simple $\text{O}-\text{H} \cdots \text{Cl}$ H-bonds with the adjacent molecules via the *para* hydroxy group with $d = 2.39(4)$ Å. For the chain involving the Pt(1)-containing molecules, the intermolecular H-bond has an inserted methanol molecule. The distances, d , are 2.32(5) and 1.82 Å for $\text{H}(3) \cdots \text{Cl}(2)$ and $\text{H}(1\text{A}) \cdots \text{O}(3)$, respectively. Atoms N(1)/N(2) and Pt(1)/Pt(2) lie 0.765(9)/0.798(9) and 0.424(5)/0.364(5) Å away from the P(1)/P(2)/C(1)/C(2) or P(3)/P(4)/C(34)/C(35) planes, respectively. So, as in $6 \cdot (\text{CH}_3)_2\text{SO}$, the core 6-membered Pt–P–C–N–C–P rings adopt more chair-shaped conformations. The hinge angles across the P(1)–P(2)/P(3)–P(4) vectors are 13.44(16)/12.47(16)°. The twist angles between planes P(1)/P(2)/C(1)/C(2) or P(3)/P(4)/C(34)/C(35) and rings C(3) > C(8) or C(36) > C(41) are 88.17(19)/54.62(15)°. So, while the other geometric parameters are similar between the two molecules, this twist angle is significantly different.

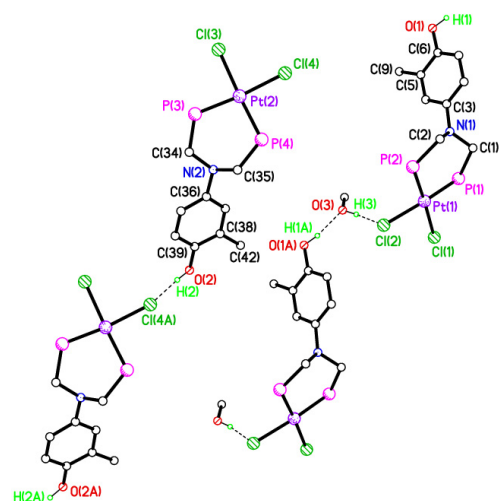


Figure 10. H-bonded packing motifs in the crystal structure of $4e \cdot \frac{1}{2}CHCl_3 \cdot \frac{1}{2}CH_3OH$. Most H atoms, two Ph groups per P atom, and the disordered chloroform of crystallisation which is not involved in any significant intermolecular interactions, are omitted for clarity. Symmetry operators are $x, y - 1, z$ and $x, y + 1, z$.

In **5c**, the amide and ring atoms from C(4) > C(11) are disordered over two sets of almost equally occupied positions. The disorder highlights two or more chain-forming possibilities for this structure, analogous to that observed in in $4e \cdot \frac{1}{2}CHCl_3 \cdot \frac{1}{2}CH_3OH$, with one possibility being simple (hydroxyl)O–H...O(amide) links (Figure 11a), while the other, shown in Figure 11b, shows an alternative, water-inserted linkage. There is also likely to be some alternation of these motifs, given the random disorder and approx. 25% occupancy observed for water atom O(3). Unlike almost all of the other structures herein, the core 6-membered Pt–P–C–N–C–P ring adopts a conformation with atoms Pt(1)/P(1)/P(1)/C(2) being in a plane and atoms C(1) and N(2) being 1.021(6) and 1.237(6) Å, respectively, away from that plane. There is no C=O...HN intermolecular H-bonding observed between molecules. Instead, the amide NH forms a bifurcated H-bond with the two neighbouring acceptor atoms N(1) and the *ortho* hydroxyl O(2) with $d = 2.37$ and 2.28 Å, respectively, while $d = 2.89$ Å for H(2)...O(1A).

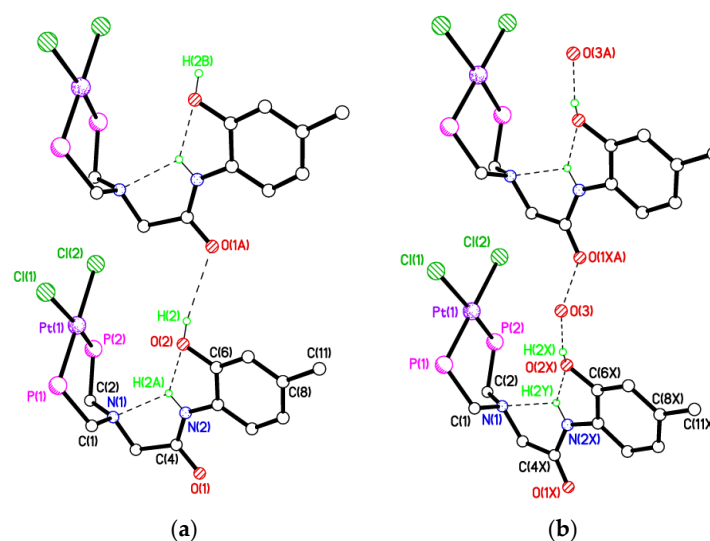


Figure 11. Most H atoms and 2 Ph groups per P atom have been omitted for clarity. **(a)** Packing motif 1 in the crystal structure of **5c**. Symmetry operator $A = x + 1, y, z$. **(b)** Packing motif 2 in the crystal structure of **5c**. The true structure is most likely an alternation of motifs 1 and 2. Symmetry operator $A = x + 1, y, z$.

In the second motif, adjacent molecules have an inserted water molecule in the H-bond pattern (Figure 11b). The amide NH again forms a bifurcated H-bond with the two neighbouring acceptor atoms N(1) and O(2X) with $d = 2.14$ and 2.25 Å, respectively, while $d = 2.89$ Å for H(2X)⋯O(3), which is a little long, and d for O(3)⋯O(1XA) = $2.21(3)$ Å, which is rather short. The distance d from water oxygen O(3) to O(1A), however, is entirely reasonable for an H-bond at 2.74 Å, suggesting a predominantly alternating pattern between the two disorder options is most likely.

Complex $5a \cdot \frac{1}{2}Et_2O$ was crystallised from a diethyl ether solution, including half a solvent molecule per complex molecule in the crystal lattice. There are two Pt complexes and two, half-occupied, Et_2O solvent molecules of crystallisation in the asymmetric unit. The packing adopted by this second complex with an *ortho* hydroxyl group is very different to **5c** (Figure 12). Here there is no intramolecular N–H⋯N H-bond, instead the *ortho* hydroxyl forms an intramolecular H-bond with the amide oxygen with $d = 1.80$ and $1.77(4)$ Å in the molecules containing Pt(1) and Pt(2), respectively. This does leave the two unique amide NH atoms free to form intermolecular interactions, which they do via highly asymmetric, bifurcated H-bonds with the coordinated chloride ligands on adjacent Pt complexes. From H(2) $d = 2.60(11)$ and $2.95(13)$ Å to Cl(3) and Cl(4), respectively, while $d = 2.52(7)$ and $3.12(15)$ Å from H(4) to Cl(1A) and Cl(2A), respectively. N(1)/N(3) and Pt(1)/Pt(2) lie $0.771(13)/0.781(14)$ and $0.349(8)/0.346(8)$ Å out of the planes P(1)/P(2)/C(1)/C(2) and P(3)/P(4)/C(37)/C(38), respectively. The twist angle between planes P(1)/P(2)/C(1)/C(2) and P(3)/P(4)/C(37)/C(38) relative to the rings C(5) > C(10) and C(41) > C(46) are $51.3(5)$ and $51.71(4)^\circ$, respectively. Hinge angles across P(1)–P(2) and P(3)–P(4) are $12.3(5)$ and $12.0(4)^\circ$, respectively. Differences between the two systems involving *ortho* hydroxyl groups are the position of the methyl ring substituent in the *meta* or *para* position, and the co-crystallised solvent being a small amount of water or Et_2O . Either, or both of these differences might account for the different intra- and intermolecular packing motifs observed. Selected hydrogen bonding parameters for $5a \cdot \frac{1}{2}Et_2O$ are shown in Table 9.

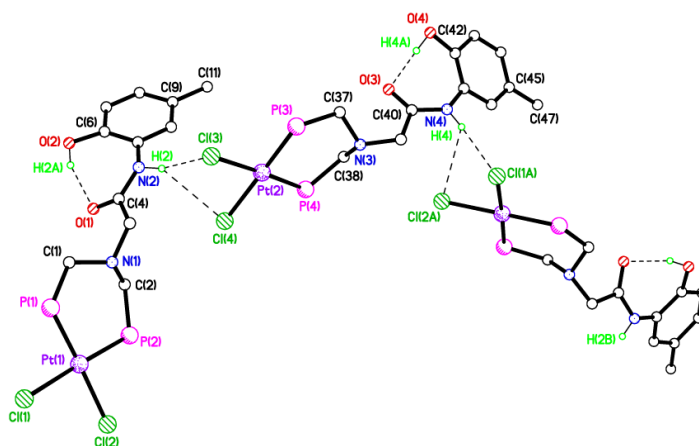


Figure 12. Packing motif in the crystal structure of $5a \cdot \frac{1}{2}Et_2O$. Most H atoms, two Ph groups per P atom and the two, half-occupied, Et_2O molecules have been omitted for clarity.

Molecules of $5d \cdot Et_2O$ lie on a mirror plane, passing through Pt(1), between pairs of P and Cl atoms, and including the atoms from N(1) to the terminal hydroxy-substituted ring. Again, here the amide NH is involved in the 1D chain propagation (Figure 13), forming a symmetrical bifurcated H-bond with the two coordinated chloride ligands on the adjacent molecule with $d = 2.66(15)$ Å. Supporting this is an additional (Ar)C–H(5)⋯Pt(1) interaction at 2.78 Å. The twist angle between the P(1)/P(1A)/C(1)/C(1A) plane and the ring C(4) > C(9) = 90° due to the imposed crystallographic symmetry. The hinge angle at P(1)–P(1A) = $29.5(5)^\circ$. Atoms N(1) and Pt(1) lie $0.79(2)$ and $0.782(14)$ Å away from the P(1)/P(2)/C(1)/C(2) plane, respectively. So, this is the most chair shaped core

Pt–P–C–N–C–P 6-membered ring. The *meta* hydroxyl group is not involved in the chain propagating intermolecular interactions and points into a cleft between a pair of Ph rings. It does not make an H-bond with the solvent of crystallisation.

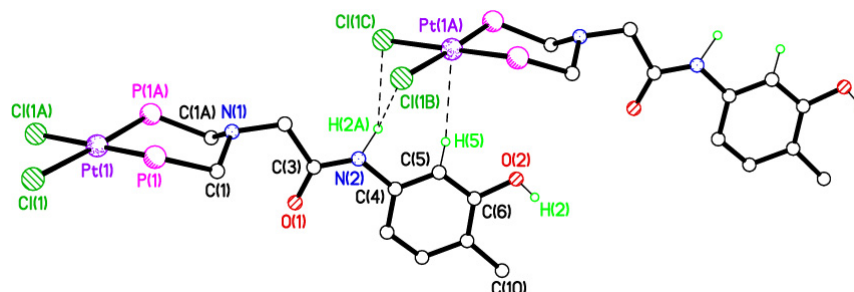


Figure 13. Packing plot of **5d**·Et₂O. Most H atoms, two Ph groups per P atom, and a disordered Et₂O molecule modelled by the Platon Squeeze procedure, are omitted for clarity. Symmetry operators: (i) for the mirror $x, y, -z + \frac{1}{2}$, (ii) for the chain direction $x + 1, y, z$.

For compound **5b**, the *para* position of the hydroxyl group facilitates 1D chain formation, forming an H-bond with one of the chloride ligands on an adjacent molecule with $d = 2.09(6)$ Å (Figure 14). The amide NH here forms the familiar, but not universal, H-bond with the amine N(1) with $d = 2.29(5)$ Å. The twist angle between the P(1)/P(2)/C(1)/C(2) plane and the ring C(5) > C(10) = $68.39(12)^\circ$. The hinge angle at P(1)–P(1A) = $4.95(10)^\circ$. Atoms N(1) and Pt(1) lie 0.810(4) and 0.164(3) Å away from the P(1)/P(2)/C(1)/C(2) plane, respectively.

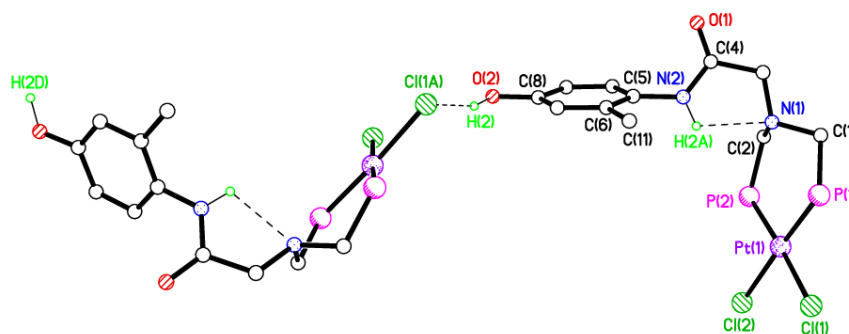


Figure 14. Packing plot in the crystal structure of **5b**. Phenyl groups and hydrogen atoms not involved in hydrogen bonding have been omitted for clarity.

3. Conclusions

In summary, we have shown that the position of the OH/CH₃ groups with respect to the N-arene, the inclusion of an amide spacer, and the solvent used in the crystallisation can dictate the solid-state packing behaviour of both non coordinated and *cis*-PtCl₂ bound diphosphine ligands. Unsurprisingly, the use of highly polar solvents (DMSO, CH₃OH) in this study has been shown to play an important role in disrupting packing behaviour. Our work reinforces the importance of substituent effects, not only those commonly associated with –PR₂ groups which may be alkyl or aryl based [37,38], but also those functional moieties positioned on the arene group of the central tertiary amine.

4. Materials and Methods

4.1. General Procedures

The synthesis of ligands **1a–e**, **2a–g**, and **3** were undertaken using standard Schlenk-line techniques and an inert nitrogen atmosphere. Ph₂PCH₂OH was prepared according to a known procedure [39]. All coordination reactions were carried out in air, using reagent grade quality solvents. The compound PtCl₂(η⁴-cod) (cod = cycloocta-1,5-diene) was

prepared according to a known procedure [40]. All other chemicals were obtained from commercial sources and used directly without further purification

4.2. Instrumentation

Infrared spectra were recorded as KBr pellets on a Perkin-Elmer Spectrum 100S (4000–250 cm^{-1} range) Fourier-Transform spectrometer. ^1H NMR spectra (400 MHz) were recorded on a Bruker DPX-400 spectrometer with chemical shifts (δ) in ppm to high frequency of $\text{Si}(\text{CH}_3)_4$ and coupling constants (J) in Hz. $^{31}\text{P}\{^1\text{H}\}$ NMR (162 MHz) spectra were recorded on a Bruker DPX-400 spectrometer with chemical shifts (δ) in ppm to high frequency of 85% H_3PO_4 . NMR spectra were measured in CDCl_3 or $(\text{CD}_3)_2\text{SO}$ at 298 K. Elemental analyses (Perkin-Elmer 2400 CHN Elemental Analyser) were performed by the Loughborough University Analytical Service within the Department of Chemistry.

4.3. Preparation of Ligands 1a–e, 2a–g, and 3

The following general procedure was used for the synthesis of **1a–e**, **2a–g**, and **3**. A mixture of $\text{Ph}_2\text{PCH}_2\text{OH}$ (2 equiv.) and the appropriate amine (1 equiv.) in CH_3OH (20 mL) was stirred under N_2 for 24 h. The volume of the solution was evaporated to ca. 2–3 mL, under reduced pressure, to afford the desired ligands which were collected by suction filtration (except **2a–c**) and dried *in vacuo*. Isolated yields in range 38–97%. Characterising details are given in Table 1.

4.4. Preparation of cis-Dichloroplatinum(II) Phosphine Complexes 4a–e, 5a–g, and 6

The following general procedure was used for the synthesis of **4a–e**, **5a–g**, and **6**. To a solution of $\text{PtCl}_2(\eta^4\text{-cod})$ (1 equiv.) in CH_2Cl_2 (5 mL) was added a solution of the appropriate ligand (1 equiv.) in CH_2Cl_2 (5 mL). The colourless (or pale yellow) solution was stirred for 30 min at r.t., evaporated to ca. 2–3 mL under reduced pressure, and diethyl ether (10 mL) added. The solids were collected by suction filtration and dried *in vacuo*. Isolated yields in range 73–99%. Characterising details are given in Table 4.

4.5. Single Crystal X-ray Crystallography

Suitable crystals of **1a**, **1b**· CH_3OH , **2f**· CH_3OH , and **3** were obtained by slow evaporation of a CH_3OH solution whereas **2g** was obtained by vapour diffusion of Et_2O into a $\text{CDCl}_3/\text{CH}_3\text{OH}$ solution. Crystals of **4b**· $(\text{CH}_3)_2\text{SO}$, **5a**· $\frac{1}{2}\text{Et}_2\text{O}$, **5b**, and **5c**· $\frac{1}{4}\text{H}_2\text{O}$ were obtained by slow diffusion of Et_2O into a $\text{CDCl}_3/(\text{CH}_3)_2\text{SO}/\text{CH}_3\text{OH}$ solution. Slow diffusion of hexanes [for **6**· $(\text{CH}_3)_2\text{SO}$] into a $\text{CDCl}_3/(\text{CH}_3)_2\text{SO}$ solution or vapour diffusion of Et_2O into a $\text{CHCl}_3/(\text{CH}_3)_2\text{SO}/\text{CH}_3\text{OH}$ [for **4c**· CHCl_3 , **4e**· $\frac{1}{2}\text{CHCl}_3$ · $\frac{1}{2}\text{CH}_3\text{OH}$] or $\text{CH}_2\text{Cl}_2/\text{CH}_3\text{OH}$ (for **5d**· Et_2O). Slow evaporation of a $\text{CH}_2\text{Cl}_2/\text{Et}_2\text{O}/\text{hexanes}$ solution gave suitable crystals of **4d**· $\frac{1}{2}\text{Et}_2\text{O}$. Tables 2, 5 and 6 summarise the key data collection and structure refinement parameters. Diffraction data for compounds **1a**, **1b**· CH_3OH , **2f**· CH_3OH , **3**, **4b**· $(\text{CH}_3)_2\text{SO}$, **4c**· CHCl_3 , **4d**, **4e**· $\frac{1}{2}\text{CHCl}_3$ · $\frac{1}{2}\text{CH}_3\text{OH}$, **5d**· Et_2O , and **6**· $(\text{CH}_3)_2\text{SO}$, were collected using a Bruker or Bruker-Nonius APEX 2 CCD diffractometer using graphite-monochromated $\text{Mo-K}\alpha$ radiation. Data for compounds **5b** and **5c**· $\frac{1}{4}\text{H}_2\text{O}$, were collected using a Bruker APEX 2 CCD diffractometer using synchrotron radiation at Daresbury SRS Station 9.8 or 16.2 SMX for **5a**· $\frac{1}{2}\text{Et}_2\text{O}$. Data for compound **2g** was collected using a Bruker SMART 1000 CCD diffractometer using graphite-monochromated $\text{Mo-K}\alpha$ radiation. All structures were solved by direct methods [except structures **4b**· $(\text{CH}_3)_2\text{SO}$, **5a**· $\frac{1}{2}\text{Et}_2\text{O}$, and **5b** which were solved using Patterson synthesis] and refined by full-matrix least-squares methods on F^2 . All CH atoms were placed in geometrically calculated positions and were refined using a riding model (aryl C–H 0.95 Å, methyl C–H 0.98 Å, methylene C–H 0.99 Å). Where data quality allowed, OH and NH atom coordinates and U_{iso} were freely refined, or refined with mild geometrical restraints; otherwise, they were placed geometrically with $\text{O/N-H} = 0.84$ Å. $U_{\text{iso}}(\text{H})$ values were set to be 1.2 times U_{eq} of the carrier atom for aryl CH and NH , and 1.5 times U_{eq} of the carrier atom for OH and CH_3 . Throughout the text and tabulated data, where H atom geometry does not include a SU, the coordinates were

constrained. Unless stated, all structural determinations proceeded without the need for restraints or disorder modelling. Where disorder was modelled it was supported with appropriate geometrical and U value restraints. In **1b**·CH₃OH, the methanol was modelled as disordered over two equally occupied sets of positions. In **2f**·CH₃OH the methanol was modelled using the Platon Squeeze procedure [41]. Compound **3** was found to contain a disordered methanol and was modelled over two sets of positions, each at half weight. In **4d**· $\frac{1}{2}$ Et₂O, atoms C(1) > C(7) and N(1) were modelled with U value restraints. The Et₂O was modelled using Platon Squeeze due to significant disorder. In **4e**· $\frac{1}{2}$ CHCl₃· $\frac{1}{2}$ CH₃OH the chloroform molecule was modelled over two sets of positions with major occupancy 57.1(7)%. Restraints were applied to that molecule and also ring C(55) > C(60). In **5a**· $\frac{1}{2}$ Et₂O three Ph rings were modelled as disordered over two sets of positions with occupancies close to 50%. Restraints were applied to these rings and also the two half-occupancy Et₂O solvent molecules of crystallisation. In **5c**· $\frac{1}{4}$ H₂O, atoms Cl(1) and C(3) > C(11), O(1), O(2) and N(1) were modelled as split over two sets of positions with major occupancy 56(4) and 50.9(6)%, respectively and restraints were applied. In **5d**·Et₂O the Et₂O was modelled as a diffuse area of electron density by the Platon Squeeze procedure and restraints were applied to atoms C(1) > C(10), C(11) > C(22) and N(2) O(2). In **6**·(CH₃)₂SO the DMSO was modelled with restraints as disordered over two sets of positions with major component 71.0(5)% and with C(33) coincident for both components Programs used during data collection, refinement and production of graphics were Bruker SMART, Bruker APEX 2, SAINT, SHELXTL, COLLECT, DENZO and local programs [41–51]. CCDC 2101643–2101656 contain the supplementary crystallographic data for this paper. These data can be obtained free of charge from The Cambridge Crystallographic Data Centre via www.ccdc.cam.ac.uk/structures (accessed on 3 November 2021).

Author Contributions: Conceptualisation, M.B.S.; synthesis and characterisation of the compounds, N.M.S.-B., P.D.; single crystal X-ray crystallography, N.M.S.-B., M.R.J.E.; writing-original draft preparation, M.B.S.; writing-review and editing, M.R.J.E., M.B.S. All authors have read and agreed to the published version of the manuscript.

Funding: This research received no external funding.

Institutional Review Board Statement: Not applicable.

Informed Consent Statement: Not applicable.

Data Availability Statement: Not applicable.

Acknowledgments: We thank the EPSRC Centre for Doctoral Training in Embedded Intelligence under grant reference EP/L014998/1 for financial support (PD). Johnson Matthey are acknowledged for their kind donation of precious metals and the UK National Crystallography Service at the University of Southampton for three of the data collections. The STFC is thanked for the allocation of beam time at Daresbury Laboratory.

Conflicts of Interest: The authors declare no conflict of interest.

Sample Availability: Samples of the compounds in this article are not available from the authors.

References

1. Lehn, J.-M. Supramolecular Chemistry-Scope and Perspectives. Molecules, Supermolecules, and Molecular Devices (Nobel Lecture). *Angew. Chem. Int. Ed. Engl.* **1988**, *27*, 89–112. [CrossRef]
2. Jongkind, L.J.; Caumes, X.; Hartendorp, A.P.T.; Reek, J.N.H. Ligand Template Strategies for Catalyst Encapsulation. *Acc. Chem. Res.* **2018**, *51*, 2115–2128. [CrossRef] [PubMed]
3. James, S.L. Phosphines as building blocks in coordination-based self-assembly. *Chem. Soc. Rev.* **2009**, *38*, 1744–1758. [CrossRef]
4. Breit, B. Supramolecular Approaches to Generate Libraries of Chelating Bidentate Ligands for Homogeneous Catalysis. *Angew. Chem. Int. Ed.* **2005**, *44*, 6816–6825. [CrossRef] [PubMed]
5. Daubignard, J.; Detz, R.J.; de Bruin, B.; Reek, J.N.H. Phosphine Oxide Based Supramolecular Ligands in the Rhodium-Catalysed Asymmetric Hydrogenation. *Organometallics* **2019**, *38*, 3961–3969. [CrossRef]
6. Koshti, V.S.; Sen, A.; Shinde, D.; Chikkali, S.H. Self-assembly of P-chiral supramolecular phosphines on rhodium and direct evidence for Rh-catalyst-substrate interactions. *Dalton Trans.* **2017**, *46*, 13966–13973. [CrossRef]

7. Vasseur, A.; Membrat, R.; Palpacelli, D.; Giorgi, M.; Nuel, D.; Giordano, L.; Martinez, A. Synthesis of chiral supramolecular bisphosphinite palladacycles through hydrogen transfer-promoted self-assembly process. *Chem. Commun.* **2018**, *54*, 10132–10135. [[CrossRef](#)] [[PubMed](#)]
8. Romero-Nieto, C.; de Cózar, A.; Regulska, E.; Mullenix, J.B.; Rominger, F.; Hindenberg, P. Controlling the molecular arrangement of racemates through weak interactions: The synergy between p-interactions and halogen bonds. *Chem. Commun.* **2021**, *57*, 7366–7369. [[CrossRef](#)] [[PubMed](#)]
9. Carreras, L.; Serrano-Torné, M.; van Leeuwen, P.W.N.M.; Vidal-Ferran, A. XBphos-Rh: A halogen-bond assembled supramolecular catalyst. *Chem. Sci.* **2018**, *9*, 3644–3648. [[CrossRef](#)]
10. García-Márquez, A.; Frontera, A.; Roisnel, T.; Gramage-Doria, R. Ultrashort H^{d+} ⋯ H^{d-} intermolecular distance in a supramolecular system in the solid state. *Chem. Commun.* **2021**, *57*, 7112–7115. [[CrossRef](#)]
11. Blann, K.; Bollmann, A.; Brown, G.M.; Dixon, J.T.; Elsegood, M.R.J.; Raw, C.R.; Smith, M.B.; Tenza, K.; Willemse, A.; Zweni, P. Ethylene oligomerisation chromium catalysts with unsymmetrical PCNP ligands. *Dalton Trans.* **2021**, *50*, 4345–4354. [[CrossRef](#)] [[PubMed](#)]
12. De' Ath, P.; Elsegood, M.R.J.; Halliwell, C.A.G.; Smith, M.B. Mild intramolecular P-C(sp³) bond cleavage in bridging diphosphine complexes of Ru^{II}, Rh^{III}, and Ir^{III}. *J. Organomet. Chem.* **2021**, *937*, 121704. [[CrossRef](#)]
13. Smith, M.B.; Dale, S.H.; Coles, S.J.; Gelbrich, T.; Hursthouse, M.B.; Light, M.E.; Horton, P.N. Hydrogen bonded supramolecular assemblies based on neutral square-planar palladium(II) complexes. *CrystEngCommun* **2007**, *9*, 165–175. [[CrossRef](#)]
14. Smith, M.B.; Dale, S.H.; Coles, S.J.; Gelbrich, T.; Hursthouse, M.B.; Light, M.E. Isomeric dinuclear gold(I) complexes with highly functionalised ditertiary phosphines: Self-assembly of dimers, rings and 1-D polymeric chains. *CrystEngCommun* **2006**, *8*, 140–149. [[CrossRef](#)]
15. Dann, S.E.; Durran, S.E.; Elsegood, M.R.J.; Smith, M.B.; Staniland, P.M.; Talib, S.; Dale, S.H. Supramolecular chemistry of half-sandwich organometallic building blocks based on RuCl₂(p-cymene)Ph₂PCH₂Y. *J. Organomet. Chem.* **2006**, *691*, 4829–4842. [[CrossRef](#)]
16. Durran, S.E.; Smith, M.B.; Slawin, A.M.Z.; Gelbrich, T.; Hursthouse, M.B.; Light, M.E. Synthesis and coordination studies of new aminoalcohol functionalised tertiary phosphines. *Can. J. Chem.* **2001**, *79*, 780–791. [[CrossRef](#)]
17. Jiang, M.-S.; Tao, Y.-H.; Wang, Y.-W.; Lu, C.; Young, D.J.; Lang, J.-P.; Ren, Z.-G. Reversible Solid-State Phase Transitions between Au-P Complexes Accompanied by Switchable Fluorescence. *Inorg. Chem.* **2020**, *59*, 3072–3078. [[CrossRef](#)]
18. Pandey, M.K.; Kunchur, H.S.; Mondal, D.; Radhakrishna, L.; Kote, B.S.; Balakrishna, M.S. Rare Au ⋯ H Interactions in Gold(I) Complexes of Bulky Phosphines Derived from 2,6-Dibenzhydryl-4-methylphenyl Core. *Inorg. Chem.* **2020**, *59*, 3642–3658. [[CrossRef](#)] [[PubMed](#)]
19. Bálint, E.; Tajti, A.; Tripolszky, A.; Keglevich, G. Synthesis of platinum, palladium and rhodium complexes of α-aminophosphine ligands. *Dalton Trans.* **2018**, *47*, 4755–4778. [[CrossRef](#)] [[PubMed](#)]
20. Zhang, Y.-P.; Zhang, M.; Chen, X.-R.; Lu, C.; Young, D.J.; Ren, Z.-G.; Lang, J.-P. Cobalt(I) and Nickel(II) Complexes of a PNN Type Ligand as Photoenhanced Electrocatalysts for the Hydrogen Evolution Reaction. *Inorg. Chem.* **2020**, *59*, 1038–1045. [[CrossRef](#)]
21. Hou, R.; Huang, T.-H.; Wang, X.-J.; Jiang, X.-F.; Ni, Q.-L.; Gui, L.-C.; Fan, Y.-J.; Tan, Y.-L. Synthesis, structural characterisation and luminescent properties of a series of Cu(I) complexes based on polyphosphine ligands. *Dalton Trans.* **2011**, *40*, 7551–7558. [[CrossRef](#)]
22. Wang, X.-J.; Gui, L.-C.; Ni, Q.-L.; Liao, Y.-F.; Jiang, X.-F.; Tang, L.-H.; Zhang, Z.; Wu, Q. p-Stacking induced complexes with Z-shape motifs featuring a complementary approach between electron-rich arene diamines and electron-deficient aromatic N-heterocycles. *CrystEngComm* **2008**, *10*, 1003–1010. [[CrossRef](#)]
23. Au, R.H.W.; Jennings, M.C.; Puddephatt, R.J. Supramolecular Organoplatinum(IV) Chemistry: Sequential Introduction of Amide Hydrogen Bonding Groups. *Organometallics* **2009**, *28*, 3754–3762. [[CrossRef](#)]
24. Coles, N.T.; Gasperini, D.; Provis-Evans, C.B.; Mahon, M.F.; Webster, R.L. Heterobimetallic Complexes of 1,1-Diphosphineamide Ligands. *Organometallics* **2021**, *40*, 148–155. [[CrossRef](#)]
25. Navrátil, M.; Císařová, I.; Alemayehu, A.; Škoch, K.; Štěpnička, P. Synthesis and Structural Characterisation of an N-Phosphanyl Ferrocene Carboxamide and its Ruthenium, Rhodium and Palladium Complexes. *ChemPlusChem* **2020**, *85*, 1325–1338. [[CrossRef](#)]
26. Navrátil, M.; Císařová, I.; Štěpnička, P. Intermolecular interactions in the crystal structures of chlorogold(I) complexes with N-phosphinoamide ligands. *Inorg. Chim. Acta* **2021**, *516*, 120138. [[CrossRef](#)]
27. Pachisia, S.; Kishan, R.; Yadav, S.; Gupta, R. Half-Sandwich Ruthenium Complexes of Amide-Phosphine Based Ligands: H-Bonding Cavity Assisted Binding and Reduction of Nitro-substrates. *Inorg. Chem.* **2021**, *60*, 2009–2022. [[CrossRef](#)] [[PubMed](#)]
28. Nasser, N.; Eisler, D.J.; Puddephatt, R.J. A chiral diphosphine as trans-chelate ligand and its relevance to catalysis. *Chem. Commun.* **2010**, *46*, 1953–1955. [[CrossRef](#)] [[PubMed](#)]
29. Elsegood, M.R.J.; Lake, A.J.; Smith, M.B.; Weaver, G.W. Ditertiary phosphines bearing a -N-C-C(O)-N(H)- linker and their corresponding dichloroplatinum(II) complexes. *Phosphorus Sulfur Silicon Relat. Elem.* **2019**, *194*, 540–544. [[CrossRef](#)]
30. Hoyos, O.L.; Bermejo, M.R.; Fondo, M.; García-Deibe, A.; González, A.M.; Maneiro, M.; Pedrido, R. Mn(III) complexes with asymmetrical N₂O₃Schiff bases. The unusual crystal structure of [Mn(phenglydisal-3-Br,5-Cl)(dmsol)] (H₃phenglydisal = 3-aza-N-{2-[1-aza-2-(2-hydroxyphenyl)viny]phenyl}-4-(2-hydroxyphenyl)but-3-enamide), a mononuclear single-stranded helical manganese(III) complex. *J. Chem. Soc. Dalton Trans.* **2000**, 3122–3127. [[CrossRef](#)]

31. Bermejo, M.R.; González, A.M.; Fondo, M.; García-Deibe, A.; Maneiro, M.; Sanmartín, J.; Hoyos, O.L.; Watkinson, M. A direct route to obtain manganese(III) complexes with a new class of asymmetrical Schiff base ligands. *New J. Chem.* **2000**, *24*, 235–241. [[CrossRef](#)]
32. Elsegood, M.R.J.; Smith, M.B.; Staniland, P.M. Neutral Molecular Pd₆ Hexagons Using k³-P₂O Terdentate Ligands. *Inorg. Chem.* **2006**, *45*, 6761–6770. [[CrossRef](#)] [[PubMed](#)]
33. Etter, M.C.; MacDonald, J.C.; Bernstein, J. Graph-Set Analysis of Hydrogen-Bond Patterns in Organic Crystals. *Acta Crystallogr.* **1990**, *B46*, 256–262. [[CrossRef](#)]
34. Etter, M.C. Encoding and Decoding Hydrogen-Bond Patterns of Organic Compounds. *Acc. Chem. Res.* **1990**, *23*, 120–126. [[CrossRef](#)]
35. Bernstein, J.; Davis, R.E.; Shimoni, L.; Chang, N.-L. Patterns in Hydrogen Bonding: Functionality and Graph Set Analysis in Crystals. *Angew. Chem. Int. Ed. Engl.* **1995**, *34*, 1555–1573. [[CrossRef](#)]
36. Desiraju, G.; Steiner, T. *The Weak Hydrogen Bond*; Oxford University Press: Oxford, UK, 2001.
37. Klemms, C.; Payet, E.; Magna, L.; Saussine, L.; Le Goff, X.F.; Le Floch, P. PCNCP Ligands in the Chromium-Catalysed Oligomerisation of Ethylene: Tri-versus Tetramerization. *Chem. Eur. J.* **2009**, *15*, 8259–8268. [[CrossRef](#)]
38. Walsh, A.P.; Laureanti, J.A.; Katipamula, S.; Chambers, G.M.; Priyadarshani, N.; Lense, S.; Bays, J.T.; Linehan, J.C.; Shaw, W.J. Evaluating the impacts of amino acids in the second and outer coordination spheres of Rh-bis(diphosphine) complexes for CO₂ hydrogenation. *Faraday Discuss.* **2019**, *215*, 123–140. [[CrossRef](#)] [[PubMed](#)]
39. Hellman, H.; Bader, J.; Birkner, H.; Schumacher, O. Hydroxymethyl-phosphine, Hydroxymethyl-phosphoniumsalze und Chlormethyl-phosphoniumsalze. *Justus Liebigs Ann. Chem.* **1962**, *659*, 49–56. [[CrossRef](#)]
40. McDermott, J.X.; White, J.F.; Whitesides, G.M. Thermal Decomposition of Bis(phosphine)platinum(II) Metallocycles. *J. Am. Chem. Soc.* **1976**, *98*, 6521–6528. [[CrossRef](#)]
41. Spek, A.L. PLATON SQUEEZE: A tool for the calculation of the disordered solvent contribution to the calculated structure factors. *Acta Crystallogr. Sect. C-Struct. Chem.* **2015**, *71*, 9–18. [[CrossRef](#)]
42. Sluis, P.v.d.; Spek, A.L. BYPASS: An effective method for the refinement of crystal structures containing disordered solvent regions. *Acta Crystallogr.* **1990**, *A46*, 194–201. [[CrossRef](#)]
43. Bruker SMART Version 5.611; Bruker AXS Inc.: Fitchburg, WI, USA, 2001.
44. Area-Detector Integration Software, APEX-II, Version V1; Bruker-Nonius: Madison, WI, USA, 2004.
45. Denzo, Z.; Otwinowski, W. Processing of X-ray diffraction data in oscillation mode, *Methods in Enzymology*. In *Macromolecular Crystallography*; Carter, C.W., Jr., Sweet, R.M., Eds.; Academic Press: Cambridge, MA, USA, 1997; Volume 276, pp. 307–326.
46. Hooft, R.W.W. COLLECT: Data Collection Software; Nonius B.V.: Delft, The Netherlands, 1998.
47. SAINT Software for CCD Diffractometers; Bruker AXS Inc.: Madison, WI, USA, 2004.
48. Krause, L.; Herbst-Irmer, R.; Sheldrick, G.M.; Stalke, D.J. SADABS software. *J. Appl. Cryst.* **2015**, *48*, 3–10. [[CrossRef](#)] [[PubMed](#)]
49. Sheldrick, G.M. Crystal structure refinement with SHELXL. *Acta Crystallogr. Sect.* **2015**, *A71*, 3–8. [[CrossRef](#)]
50. Sheldrick, G.M. A short history of SHELX. *Acta Crystallogr. Sect.* **2008**, *A64*, 112–122. [[CrossRef](#)] [[PubMed](#)]
51. Sheldrick, G.M. *SHELXTL User Manual, Version 6.12*; Bruker AXS Inc.: Madison, WI, USA, 2001.